LEARNING GRID-LIKE UNITS WITH VECTOR REPRESENTATION OF SELF-POSITION AND MATRIX REPRESENTATION OF SELF-MOTION

Anonymous authors
Paper under double-blind review

ABSTRACT

This paper proposes a simple model for learning grid-like units for spatial awareness and navigation. In this model, the self-position of the agent is represented by a vector, and the self-motion of the agent is represented by a block-diagonal matrix. Each component of the vector is a unit (or a cell). The model consists of the following two sub-models. (1) Motion sub-model. The movement from the current position to the next position is modeled by matrix-vector multiplication, i.e., multiplying the matrix representation of the motion to the current vector representation of the position in order to obtain the vector representation of the next position. (2) Localization sub-model. The adjacency between any two positions is a monotone decreasing function of their Euclidean distance, and the adjacency is modeled by the inner product between the vector representations of the two positions. Both sub-models can be implemented by neural networks. The motion sub-model is a recurrent network with dynamic weight matrix, and the localization sub-model is a feedforward network. The model can be learned by minimizing a loss function that combines the loss functions of the two sub-models. The learned units exhibit grid-like patterns (as well as stripe patterns) in all 1D, 2D and 3D environments. The learned model can be used for path integral and path planning. Moreover, the learned representation is capable of error correction.

1 INTRODUCTION

Since the discovery of grid cells in the navigation system of the mammalian brain (Hafting et al. (2005); Fyhn et al. (2008); Yartsev et al. (2011); Killian et al. (2012); Jacobs et al. (2013); Doeller et al. (2010)), many mathematical and computational models (Burak & Fiete (2009); Sreenivasan & Fiete (2011); Blair et al. (2007); de Almeida et al. (2009)) have been proposed to explain the formation and function of grid cells. Recently, deep learning models (Banino et al. (2018); Cueva & Wei (2018)) have been proposed to learn the grid-like units for navigation. Such models consist of two sub-models. One is the motion sub-model, which is in the form of a recurrent neural network, to capture the change of the latent vector along the trajectory of the agent. The other is the localization sub-model, which is in the form of a feedforward neural network, to model the mapping from the latent vector to the position of the agent. The models of grid-like units can be used for two important tasks in navigation. One is path integral (Hafting et al. (2005); Fiete et al. (2008); McNaughton et al. (2006)) whose goal is to estimate the self-position of the agent given a sequence of it's self-motions. The other is path planning (Fiete et al. (2008); Erdem & Hasselmo (2012); Bush et al. (2015)) whose goal is to plan a sequence of self-motions in order to reach a given target destination. The model can be learned by supervised learning that minimizes the prediction error between the predicted position and the true position in path integral. It can also be learned by reinforcement learning for path planning.

Our work is inspired by the recent deep learning models on grid cells. However, instead of further generalizing and extending them, or making connections to the neuroscience of the grid cells, we seek to find a simple and explicit model for learning grid-like units for spatial awareness and navigation. Our motivation is that for such a basic system, we may only need a simple model that consists of one layer networks. The motion sub-model is a one layer recurrent network with dynamic weight matrix, while the localization model is a one layer linear feedforward network.

Specifically, in our model, the self-position of the agent is represented by a vector of a certain dimensionality, where each component of the vector is a unit (or a cell). The self-motion of the agent is represented by a matrix that depends on the self-motion or displacement. When the agent moves from the current position to the next position, the vector representation undergoes a linear transformation, where the vector representation of the next position is obtained by multiplying the matrix of the self-motion to the vector representation of the current position. For the sake of estimation accuracy and computational efficiency, we assume that the self-motion matrix is block diagonal. That is, we partition the components of the vector into different blocks of sub-vectors, with each block consisting of a small number of units (e.g., 6 units), and each block undergoes its own linear transformation by a multiplication of a small matrix. In other words, the dynamics of the blocks are disentangled.

In addition to the above motion sub-model in the form of vector-matrix multiplication, we have the localization sub-model which also embraces simplicity. For any two positions, we define their adjacency as a kernel function of their Euclidean distance. This kernel function is given to the learning algorithm. It has the maximal value 1 at zero distance and decreases monotonically to 0 as the distance increases. In the localization sub-model, the adjacency between any two positions is given by the inner product between their vector representations. This localization model enables the agent to decode the position of a vector for the purpose of the path integral. Specifically, we compute the inner product between the given vector and the vectors of all the possible positions to obtain a heat map for all the possible positions, where the maximum is the inferred position. This heat map may inform the place cells, together with visual cues of the environment. The model also enables the agent to do path planning by a simple steepest ascent algorithm that sequentially maximizes the adjacency to the destination. Since the adjacency is 1 at zero distance, the vector is of unit norm, and the self-motion is represented by a rotation of this unit vector on a high-dimensional sphere, where the arc length on the sphere informs the Euclidean distance in the original 2D space.

Both the motion and the localization sub-models can be viewed as simple neural networks, with the motion model being a one layer recurrent network with disentangled blocks and with dynamic weight matrix, while the localization model being a feedforward one layer linear network. Thus, our model is a drastic simplification of existing deep learning models of grid cells, without inserting any artificial assumptions such as Fourier basis or clock arithmetics, etc. (Blair et al. (2007); de Almeida et al. (2009))

We show that the learned units of the vector representation exhibit grid-like patterns as well as stripe patterns. We also show that the learned model can do path integral and path planning. Moreover, the learned representation is capable of error correction (appendix D.1).

The following are the contributions of our work. (1) We propose a novel model for learning grid-like units for navigation. The model has explicit representations of self-position and self-motion in terms of vector and matrix. (2) We show that the learned units exhibit periodic grid-like or strip patterns. (3) We show that the learned model can be used for path integrals. (4) We show that the learned model can perform path planning in the form of a simple steepest ascent algorithm. (5) We show that the learned representation is tolerant of additive and drop out errors. (6) We show that the model can be generalized to 1D and 3D environments, and learn meaningful grid-like patterns. The learned model can also be used for path integral and path planning.

2 Related work

Our work is inspired by recent deep learning models on grid cells (Banino et al. (2018); Cueva & Wei (2018)). However, our model is much simpler and more explicit than existing models. Our model only consists of one layer recurrent network and feedforward network, with highly interpretable sub-models of motion and localization. It is a simple and natural model without adding artificial components such as Fourier basis.

Compared to previous computational models on grid cells, our model only assumes one layer networks, without making assumptions such as Fourier plane waves or clock arithmetics (Blair et al. (2007); de Almeida et al. (2009)). As such, our goal is to find a simple loss function to learn the system.

The assumption of disentangled blocks in our model is related to the modular organization of grid cells in neuroscience (Stensola et al. (2012)), where a module refers to a region of grid cells where all cells share identical grid scale and orientation. Similarly, our result shows that within the same block, the learned units exhibit similar scales and orientations.

Similar to word2vec (Mikolov et al. (2013)), the vector representation imodularn our method may be called a place2vec. In word2vec, the inner product of two vectors measures the similarity of the words. In place2vec, the inner product of two vectors measures the adjacency of two positions.

Our model and the associated loss function is connected to several well-known machine learning methods. The representation of the adjacency kernel between two positions by the inner product between their vector representations reminds us the kernel trick in support vector machine (Cortes & Vapnik (1995)), where the adjacency is the kernel function, and the vector is a high-dimensional representation of the 2D input. The difference is that in kernel machines, the high-dimensional vector is implicit, while in our work, we aim to learn the vector representation explicitly. The explicit representation of the kernel function in terms of inner product between vectors is related to symmetric matrix factorization (Lee & Seung (1999)), which is in turn related to spectral clustering (Ng et al. (2002)) and kernel k-means (Dhillon et al. (2004)). The motion sub-model is related to local linear embedding (Roweis & Saul (2000)), except that the vectors are related by matrix representations of self-motion.

In representation theory in mathematics (Fulton & Harris (2013)), the group elements are represented by matrices acting on the vectors. We learn a special system of representation for representing self-position and self-motion.

3 MODEL

Consider an agent navigating within a domain $D = [0, 1] \times [0, 1]$. We can discretize D into an $N \times N$ lattice. Let $x = (x_1, x_2) \in D$ be the self-position of the agent. Suppose the agent wants to represent its self-position by a d-dimensional hidden vector $v(x)$. We introduce two sub-models.

3.1 MOTION SUB-MODEL

Suppose at a position x, the self-motion is Δx, so that the agent moves to $x + \Delta x$ after one step. We assume that

$$v(x + \Delta x) = M(\Delta x)v(x), \tag{1}$$

where $M(\Delta x)$ is a $d \times d$ matrix that depends on Δx. While $v(x)$ is the vector representation of the self-position x, $M(\Delta x)$ is the matrix representation of the self-motion Δx. As we will show below, $|v(x)| = 1$ for all x, thus $M(\Delta x)$ is a rotation matrix, and the self-motion is represented by a rotation in the d-dimensional sphere. We can illustrate the motion model by the following diagram:

$$\begin{array}{cccc} \text{Motion :} & x_t & \xrightarrow{+\Delta x} & x_{t+1} \\ & \downarrow & \downarrow & \downarrow \\ & v(x_t) & \xrightarrow{M(\Delta x)\times} & v(x_{t+1}) \end{array} \tag{2}$$

Both $v(x)$ and $M(\Delta x)$ are to be learned.

For the sake of estimation accuracy and computational efficiency, we further assume that $M(\Delta x)$ is block diagonal, i.e., we can divide $v = (v^{(k)}, k = 1, ..., K)$ into K blocks of sub-vectors, and $v^{(k)}(x + \Delta x) = M^{(k)}(\Delta x)v^{(k)}(x)$. That is, the vector v consists of sub-vectors, each of which rotates in its own subspace.

We can learn a separate motion matrix M for each Δx within a limited range. Because of the block-diagonal form of M, we can afford to learn such motion matrices separately. However, we can also learn a parametric model for M. To this end, we can further parametrize $M = I + \tilde{M}(\Delta x)$ such that each element of $\tilde{M}(\Delta x)$ is a quadratic (or polynomial) function of $\Delta x = (\Delta x_1, \Delta x_2)$:

$$\tilde{M}_{ij}(\Delta x) = \beta_{ij}^{(1)}\Delta x_1 + \beta_{ij}^{(2)}\Delta x_2 + \beta_{ij}^{(11)}\Delta x_1^2 + \beta_{ij}^{(22)}\Delta x_2^2 + \beta_{ij}^{(12)}\Delta x_1\Delta x_2, \tag{3}$$

where the coefficients β are to be learned. The above may be considered a second-order Taylor expansion which is expected to be accurate for small Δx.

In this model, we assume the motion Δx to be allocentric. However, the model can be generalized to handle egocentric motion (Burgess (2006)), in the sense that we decompose the egocentric motion into head direction change and scalar motion, and learn a system for each of them. This corresponds to the modeling of both head direction cells and grid cells. Please refer to appendix C for the details.

The motion model can be considered a linear recurrent neural network (RNN). However, if we are to interpret M as the weight matrix, then the weight matrix is dynamic because it depends on the motion Δx. One may implement it by discretizing Δx, so that we have a finite set of Δx, and thus a finite set of $M(\Delta x)$. Then at each time step, the RNN switches between the finite set of motion matrices. This is like the gearing operation of a multi-geared bicycle. Another implementation is to write $M(\Delta x)v = v + B^{(1)}(\Delta x_1 v) + B^{(2)}(\Delta x_2 v) + B^{(11)}(\Delta x_1^2 v) + B^{(22)}(\Delta x_2^2 v) + B^{(12)}(\Delta x_1 \Delta x_2 v)$, where the B matrices consist of the corresponding β coefficients. We first obtain new input vectors $\Delta x_1 v$, $\Delta x_2 v$, ..., $\Delta x_1 \Delta x_2 v$, and then treat $B^{(1)}, B^{(2)}, ..., B^{(12)}$ as the weight matrices operating on the new input vectors.

3.2 Localization sub-model

Let $A(x, y)$ be the adjacency measure between two positions x and y such that $A(x, y) = f(|x - y|)$, where $f(r)$ decreases monotonically as the Euclidean distance $r = |x - y|$ increases. One example of f is the Gaussian kernel $f(r) = \exp\left(-\frac{r^2}{2\sigma^2}\right)$. Another example is the exponential kernel $f(r) = \exp\left(-\frac{r}{\sigma}\right)$. As a matter of normalization, we assume $f(0) = 1$.

We assume the adjacency measure is given by the inner product between the hidden vectors

$$A(x, y) = \langle v(x), v(y) \rangle. \tag{4}$$

Since $f(0) = 1$, $|v(x)| = 1$ for any x, and $\langle v(x), v(y) \rangle = \cos \alpha$, where α is the angle between $v(x)$ and $v(y)$. Thus for a vector v, the distance between it's position and x is $f^{-1}(\langle v, v(x) \rangle)$. Since $f(r)$ is monotonically decreasing, $h(x) = \langle v, v(x) \rangle$ gives us the heat map to decode the position of v. Let the decoded position be $\hat{x}$, then $\hat{x} = \arg\max_x \langle v, v(x) \rangle$. We can obtain the one-hot representation $\delta_{\hat{x}}$ of $\hat{x}$ by non-maximum suppression on the heat map $h(x)$.

The heat map $h(x)$ can be combined with visual feature maps to infer the position if there are visual cues. Our system can be embedded into the SLAM (simultaneous localization and mapping) system (Whyte (2006)), which is based on a state space model that consists of a dynamic sub-model for self-position due to self-motion, and an observation sub-model for the observed visual image given the self-position. We can represent the dynamic sub-model by our system, or reformulate the whole model using our scheme. We leave it to future work.

Let $V = (v(x), \forall x)$ be the $d \times N^2$ matrix, where each column is a $v(x)$. We can write the heat map of a d-dimensional vector v by a N^2-dimensional vector $h = V^\top v$, which serves to decode the position x encoded by v. Conversely, for a one-hot representation of a position x, i.e., δ_x, which is a one-hot N^2-dimensional vector, we can encode it by $v = V\delta_x$. Both the encoder and decoder can be implemented by a linear neural network with connection weights V and $V^\top$ respectively, as illustrated by the following diagram:

$$\begin{array}{llcll} \text{Localization}: & v & \xrightarrow{V^\top \times} & h & \text{(heat map and decoding to } \delta_x\text{)} \\ & \delta_x & \xrightarrow{V \times} & v(x) & \text{(encoding)} \end{array} \tag{5}$$

Note that in decoding $v \to h(x) \to \delta_x$ and encoding $\delta_x \to v$, we do not represent or operate on the 2D coordinate x explicitly, i.e., x itself is never explicitly represented, although we may use the notation x in the description of the experiments.

4 LEARNING

4.1 LOSS FUNCTION

We can learn v and M (or the β coefficients that parametrize M) by minimizing

$$\mathbb{E}_{x,y}\left[(A(x,y) - \langle v(x), v(y)\rangle)^2\right] + \lambda \mathbb{E}_{x,\Delta x}\left[\|v(x+\Delta x) - M(\Delta x)v(x)\|^2\right], \tag{6}$$

where $\lambda > 0$ is a tuning constant. The first term is the localization loss, and the second term is the motion loss. In the first expectation, we assume x and y are sampled uniformly from D. In the second expectation, we assume that x is sampled uniformly from D, while Δx is sampled uniformly within a limited range.

The above loss function can be conveniently minimized by gradient descent. We may re-parametrize $M(\Delta x)$ in a residual form $M(\Delta x) = I + \tilde{M}(\Delta x)$, and do gradient descent with respect to $\tilde{M}$. In the case where $\tilde{M}(\Delta x)$ is parameterized by a quadratic function of $\Delta x = (\Delta x_1, \Delta x_2)$, we can further back-propagate the gradient of $\tilde{M}$ to the β coeffcients.

We impose regularization terms $U(v) = \sum_{i=1}^{d}\left(\mathbb{E}_x[v_i(x)^2] - 1/d\right)^2$ to enforce uniform energy of the units for $v = (v_i(x), i = 1, ..., d)^\top$. It also helps to break the symmetry caused by the fact that the loss function is invariant under the transformation $v(x) \to Qv(x), \forall x$, where Q is an arbitrary $d \times d$ orthogonal matrix.

The motion loss $\mathbb{E}_{x,\Delta x}\left[\|v(x+\Delta x) - M(\Delta x)v(x)\|^2\right]$ is a single-step loss. It can be generalized to multi-step loss

$$\mathbb{E}_{x,\Delta x_1,...\Delta x_T}\left[\|v(x+\Delta x_1 + ... + \Delta x_T) - M(\Delta x_T)...M(\Delta x_1)v(x)\|^2\right], \tag{7}$$

where $(\Delta x_t, t = 1, ..., T)$ is a sequence of T steps of displacements.

4.2 IMPLEMENTATION DETAILS

We obtain inputs for learning the model by simulating agent trajectories with duration $\tilde{T}$ in the square domain D. D is discretized into a 40×40 lattice and the agent is only allowed to move on the lattice. The agent starts at a random location x_0. At each time step t, a small motion Δx_t (≤ 3 grids in each direction) is randomly sampled with the restriction of not leading the agent outside the boundary, resulting in a simulated trajectory $\{x_0 + \sum_{i=1}^{t} \Delta x_i\}_{t=1}^{\tilde{T}}$. $\tilde{T}$ is set to $1,000$ to obtain trajectories that are uniformly distributed over the whole area. It is worth mentioning that although the trajectories used for training are restricted to the lattice and with small motions, in Section 5.4 we show that the learned model can be easily generalized to handle continuous positions and large motions. In training, pairs of locations (x, y) are randomly sampled from each trajectory as the input to the localization loss, while consecutive position sequences $(x, \Delta x_t, t = 1, ..., T)$ are randomly sampled as the input to the motion loss term, with length specified by T (which is usually much smaller than the whole length of the trajectory $\tilde{T}$).

The model is trained with Adam optimizer (Kingma & Ba (2014)) (lr $= 0.03$) for $6,000$ iterations. A batch of $30,000$ examples (i.e., (x, y) and $(x, \Delta x_t, t = 1, ..., T)$) is sampled from the simulated trajectories at each learning iteration as the input to the loss function. λ is set to 0.1 to balance the magnitude of the two loss terms. The weight for the regularization term is set to $5,000$. In the later stage of learning ($\geq 4,000$ iterations), $|v(x)| = 1$ is enforced by projected gradient descent, i.e., normalizing each $v(x)$ after the gradient descent step. We use 16 blocks of units with block size 6, resulting in 96 units in total.

5 EXPERIMENTS

First, we conduct experiments on simulation data to learn the units $v(x)$ and motion matrices $M(\Delta x)$ parametrized by the β coefficients. Then, we show that the learned representation can perform path integral and path planning tasks.

5.1 LEARNING SINGLE BLOCKS: HEXAGON PATTERNS AND METRICS

We begin with learning the system using a single block of units. We derive a generic local adjacency by the second order Taylor expansion. Then we show that learning with such a simple adjacency measure, grid-like patterns emerge. When block size is larger than or equal to 6, they are arranged in a very regular hexagon lattice. The patterns remain stable and are easy to learn even when the block size is large. Finally, we provide an analytical solution that helps understand the emergence of hexagon patterns.

5.1.1 LOCAL ADJACENCY AND METRIC

Consider a single block $v^{(k)}$. Assume

$$A_k(x, y) = \langle v^{(k)}(x), v^{(k)}(y)\rangle = f_k(|x - y|), \tag{8}$$

then $A(x, y) = \sum_{k=1}^{K} A_k(x, y)$, and $f(r) = \sum_{k=1}^{K} f_k(r)$.

For simplicity, let us assume we re-normalize $v^{(k)}(x)$ so that $|v^{(k)}(x)|^2 = 1$ for all x. Assume $f_k(r)$ is twice differentiable at the maximum $r = 0$, then $f'_k(0) = 0$. Let $\alpha_k = -f''_k(0)/2$, by second order Taylor expansion, $f_k(r) \approx 1 - \alpha_k r^2$ for small r, i.e., locally, we have the adjacency for a single block:

$$\begin{aligned} A_k(x, y) &= \langle v^{(k)}(x), v^{(k)}(y)\rangle = \cos\angle(v^{(k)}(x), v^{(k)}(y)) && (9)\\ &\approx 1 - \alpha_k|x - y|^2 \approx \cos(\sqrt{2\alpha_k}|x - y|). && (10)\end{aligned}$$

Thus locally the angle or arc length $\angle(v^{(k)}(x), v^{(k)}(y)) \approx \sqrt{2\alpha_k}|x - y|$, i.e., $\sqrt{2\alpha_k}$ is the metric of the block k. α_k can be either specified or learned.

5.1.2 LEARNING SINGLE BLOCKS

We learn the system using a single block of units and the generic local adjacency measure

$$A(x, y) = 1 - \alpha|x - y|^2, \;\; \forall(x, y) : |x - y| \leq \sqrt{1.5/\alpha}. \tag{11}$$

Figure 1 shows the learned units over the 40×40 lattice of x. Figure 1(a) shows the learned results with 6 units and different values of α. The learned units have obvious grid-like patterns, which are arranged in a very regular hexagon lattice. The scale or metric of the lattice is controlled by α. The units within a block have patterns with similar scale and arrangement, and different phases. Figure 1(b) shows the learned results with 100 units and $\alpha = 72$, indicating that the grid-like patterns are stable and easy to learn even when the number of units is large. When block size is 4 or 5, the learned patterns are arranged in a square lattice. Please refer to the appendix B.1 for learned units with more choices of block size.

We would like to emphasize that the local adjacency (11) is merely a second order Taylor expansion, and it assumes much less than the analytical solution that we are going to introduce.

5.1.3 ANALYTICAL SOLUTION

We provide an analytical solution. We begin the analysis by considering a single block of units and using the generic local adjacency measure $A(x, y) = 1 - \alpha|x - y|^2$, which holds only when $|x - y|$ is small. We show that when a block of 6 units is used, there exists analytical solution $v(x)$ and $M(\Delta x)$ for the system. The analytical solution has hexagon periodicity over the whole region, with the scale controlled by parameter α. We refer to α as the scaling parameter.

Theorem 1. *Let $e(x) = (e^{i\langle a_j, x\rangle}, j = 1, 2, 3)^\top$, and a_1, a_2, a_3 are three 2D vectors so that the angle between a_i and a_j is $2\pi/3$ for $\forall i \neq j$ and $|a_j| = 2\sqrt{\alpha}$ for $\forall j$. Let C be a random 3×3 complex matrix such that $C^*C = I$. Then $v(x) = Ce(x)/\sqrt{3}$, $M(\Delta x) = C\mathrm{diag}(e(\Delta x))C^*$ satisfy equation 1 $\forall x, \Delta x$, and equation 8 $\forall x, y$, approximately for small $|x - y|$.*

Proof. See appendix A. □

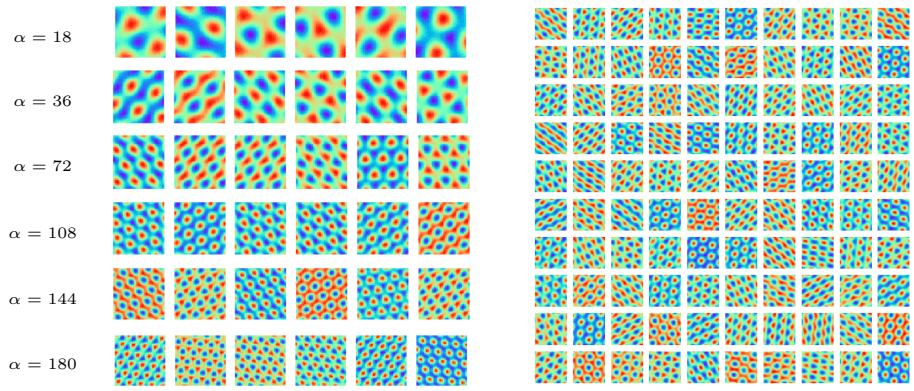

(a) Learned single block with 6 units (b) Learned single block with 100 units

Figure 1: Learned units of the vector representation using single block. (a) Learned single block with 6 units. Every row shows the learned units with a certain α. (b) Learned single block with 100 units and $\alpha = 72$.

$v(x)$ amounts to a 6-d real vector. Under the condition $|x - y| \leq \sqrt{1.5/\alpha}$, the adjacency measure $A(x, y) \approx \cos(\sqrt{2\alpha}|x - y|)$. Since the angle between a_i and a_j is $2\pi/3$ for $\forall i \neq j$, patterns of $v(x)$ over x have hexagon periodicity. Moreover, the scale of the patterns is controlled by the length of a_j, i.e., the scaling parameter α.

For multiple blocks $v = (v^{(k)}, k = 1, ..., K)$, the analytical solution exists for block size $= 6$ and a global translation invariant $A(x, y)$. See appendix A.

5.2 Learning multiple hexagon blocks and metrics

Clear hexagon patterns emerge in learning single blocks with local adjacency. However, a global adjacency is required for the agent to localize the position uniquely. Inspired by the results in section 5.1, we propose to combine the global and local adjacencies together, and learn v and M by minimizing

$$\mathbb{E}_{x,y}\left[(A(x,y) - \langle v(x), v(y)\rangle)^2\right] + \gamma \sum_k \mathbb{E}_{(x,y)\in D_{\alpha_k}}\left[(A_k(x,y) - \langle v^{(k)}(x), v^{(k)}(y)\rangle)^2\right] \quad (12)$$
$$+\lambda \mathbb{E}_{x,\Delta x}\left[\|v(x + \Delta x) - M(\Delta x)v(x)\|^2\right],$$

where λ and γ are two tuning constants. $A(x, y)$ is the global adjacency such as the Gaussian kernel, and $A_k(x, y)$ are the local adjacencies defined by equation 11. Instead of manually assigning the scaling parameters α_k, we learn α_k by gradient descent, together with v and M simultaneously. Since the local adjacency holds only when $|x - y|$ is small, at each iteration, we sample (x, y) uniformly from $D_{\alpha_k} = \{(x, y) : |x - y| \leq \sqrt{1.5/\alpha_k}\}$ for the kth expectation in the second term, where α_k are the learned paramters at the current iteration.

In Figure 2(a), we show the learned units $v(x)$ over the 40×40 lattice of x and the learned metrics α_k. A Gaussian kernel with $\sigma = 0.08$ is used for the global adjacency measure. Block size is set to 6 and each row shows the learned units belonging to the same block. Interestingly, the learned units exhibit obvious grid-like patterns, with multiple firing fields of roughly circle or ellipse shapes. The scales of the firing fields are controlled by the learned α_k. Furthermore, the firing fields are arranged in a regular hexagon lattice. Within each block, the units exhibit very similar patterns, with different phases. In (Blair et al. (2007)), the grid cell response is modeled by three cosine gratings with different orientations and phases. In our model, we learn such patterns of different scales without inserting artificial assumptions. We also try different choices of block sizes and shapes of area. When block size is 4 or 5, the learned patterns are arranged in square lattices. When block size is larger than or equals to 6, the learned patterns are arranged in hexagon lattices. The learned patterns are similar in circular and triangular shapes of area. Please refer to appendix B.2 for more results. For the motion matrix $M(\Delta x)$, we perform an ablation study where the parametrization of $M(\Delta x)$ by β coefficients and the block diagonal assumption are dropped. Please refer to appendix B.4 for the results.

We conduct quantitative analysis of the spatial activity of the learned units, using measures adopted from the neuroscience literature (Langston et al. (2010); Sargolini et al. (2006)). 76 of 96 learned units resemble grid cells, exhibiting significant hexagonal periodicity measured by gridness score. The scales and orientations of the grid-patterns, measured from the autocorrelograms of the learned units' response maps, vary among units while remain similar within each block. Interestingly, the averaged grid scales within each block is nicely proportional to the corresponding learned $1/\sqrt{\alpha_k}$. Please refer to appendix B.3 for the details.

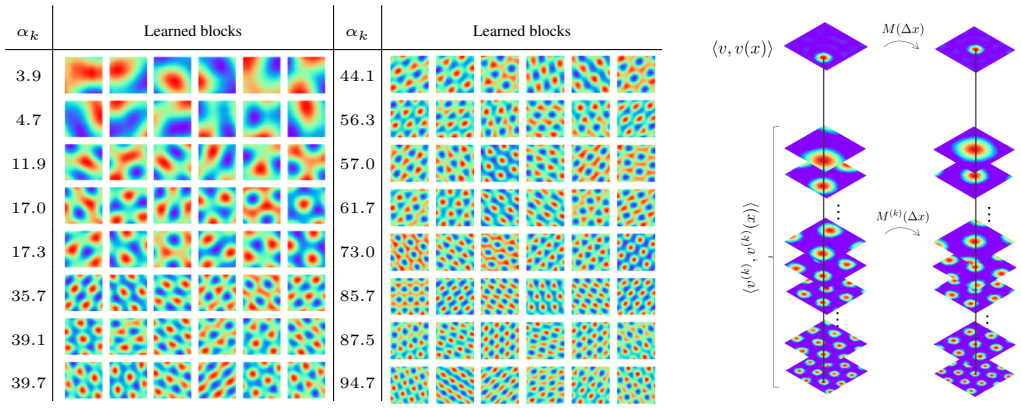

(a) Learned multiple blocks and metrics (b) Disentangled blocks

Figure 2: (a) Response maps of learned units of the vector representation and learned scaling parameters α_k. Block size equals 6 and each row shows the units belonging to the same block. (b) Illustration of block-wise activities of hidden units (where the activities are rectified to be positive).

Both localization and motion models can be interpreted as a combination of sub-blocks. Figure 2(b) provides an illustration. For the localization model, given a vector v, the heat map of a single block $\langle v^{(k)}, v^{(k)}(x)\rangle$ has periodic firing fields and cannot determine a location uniquely. However, ambiguities disappear by combing the heat maps of multiple blocks, which have firing fields of multiple scales and phases and add up to a Gaussian kernel $\langle v, v(x)\rangle$. The Gaussian kernel informs the place cell, by which the location is determined uniquely. For a motion Δx, every block rotates in its own subspace with motion matrix $M^{(k)}(\Delta x)$, resulting in phase shifting in the heat map of each single block.

Compared to Rahimi & Recht (2008) and Choromanski et al. (2018), which use random Fourier features to approximate the RBF kernel with high-dimensional input, our model is different in that (1) we learn the representation without assuming Fourier basis; (2) we use a generic local radial basis adjacency for each block; (3) we learn the local metric for each block; and more importantly (4) we have a motion sub-model.

In subsequent experiments, we only use global kernel to learn the grid cells for simplicity.

5.3 Path integral

Path integral (also referred to as dead-reckoning) is the task of inferring the self-position based on self-motion (e.g., imagine walking in a dark room). Specifically, the input to path integral is a previously determined initial position x_0 and known or estimated motion sequences $\{\Delta x_1, ..., \Delta x_T\}$, and the output is the prediction of one's current position x_T. We test our learned system on this task. We first encode the initial position x_0 as $v(x_0)$. Then, by the motion model, the hidden vector $v(x_T)$ at time T can be predicted as:

$$v(x_T) = \prod\nolimits_{t=T}^{1} M(\Delta x_t) v(x_0) = M\left(\sum\nolimits_{t=1}^{T} \Delta x_t\right) v(x_0). \tag{13}$$

That is, the learned system of $(v(x), M(\Delta x), \forall x, \Delta x)$ should satisfy the above condition. Note that this does not imply $\prod_{t=T}^{1} M(\Delta x_t) = M\left(\sum_{t=1}^{T} \Delta x_t\right)$. The above equation is true only for a spatial system of $(v(x), \forall x)$. Thus, $(v(x), M(\Delta x), \forall x, \Delta x)$ forms a whole system for spatial awareness. By the localization model, the inferred position at time T is $\hat{x}_T = \arg\max_x \langle v(x_T), v(x)\rangle$.

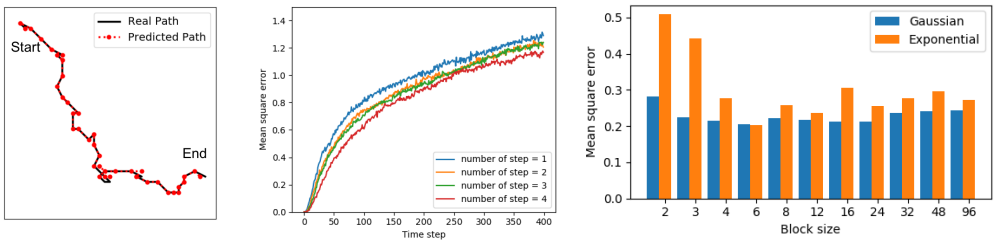

(a) Predicted path (b) MSE over time step (c) Selection of block sizes and kernels

Figure 3: (a) Path integral prediction. The black line depicts the real path while red dotted line is the predicted path by the learned model. (b) Mean square error over time step. The error is average over $1,000$ episodes. The curves correspond to different number of steps used in the multi-step motion loss. (c) Mean square error performed by models with different block sizes and different kernel types. Error is measured by number of grids.

Figure 3a shows an example of path integral result (time duration $\tilde{T} = 40$), where we use single step motion loss, unlike (Banino et al. (2018); Cueva & Wei (2018)), which train RNN or LSTM with long-term loss to fit the path integral task. Gaussian kernel with $\sigma = 0.08$ is used as the adjacency measure. We find single-step loss is sufficient for performing path integral. The mean square error remains small (~ 1.2 grid) even after 400 steps of motions (figure 3b). The error is average over $1,000$ episodes. The motion loss can be generalized to multi-step, as shown by equation 7. In Figure 3b, we show that multi-step loss can improve the performance slightly.

A question is whether the assumed block-diagonal motion matrix $M(\Delta x)$ affects the accuracy of path integral, since such assumption leads to much less parameters. In Figure 3c we compare learned models with fixed number of hidden units (96) but different block sizes. We also compare the performance of models using Gaussian kernel ($\sigma = 0.08$) and exponential kernel ($\sigma = 0.3$) as the adjacency measure in the localization model. The result shows that models with Gaussian kernel and block size ≥ 3, and with exponential kernel and block size ≥ 4 have comparative performances with the model learned without block-diagonal assumption (block size $= 96$).

5.4 Path planning

Our representation scheme $(v(x), M(\Delta x), A(x, y))$ mirrors $(x, \Delta x, |x - y|)$ used in robotics. Thus the learned representation is capable of implementing existing path planning algorithms in robotics even though our system does not have explicit coordinates in 2D (i.e., the 2D coordinates x are never explicitly represented by two neurons). We shall illustrate this point by implementing a path planning algorithm that is similar to the potential field method in robotics (Siegwart et al. (2011)), thus sharing the advantages (such as simplicity and efficiency) and disadvantages (such as not guided by a cost function on the whole path) of the latter.

Suppose the agent wants to plan a sequence of self-motions given a start position x_0 and a target destination y. In the simplest scenario, where no obstacle is involved, the agent should be able to plan direct path between x_0 and y. The global adjacency between x_0 and y serves as an attractive force, and the learned system enables the agent to do path planning by steepest ascent: (1) encoding x_0 and y to hidden vectors $v(x_0)$ and $v(y)$, and (2) sequentially maximizing the global adjacency of the current hidden vector to $v(y)$. Specifically, in the simplest scenario, suppose the hidden vector is v_t at time t, the agent chooses a motion Δx_t from a motion pool $\mathcal{M}$ by

$$\Delta x_t = \arg\max_{\Delta x \in \mathcal{M}} \langle v(y), M(\Delta x) v_t \rangle, \tag{14}$$

and then the hidden vector is updated by $v_{t+1} = M(\Delta x_t) v_t$. The planning process terminates if the global adjacency $\langle v_t, v(y) \rangle$ is close to 1 or the number of planning steps reaches a predefined maximum value.

A critical question is how to choose the motion pool $\mathcal{M}$. To augment motion candidates, we no longer restrict the motion to be on the lattice. Instead, for a small length r, we evenly divide $[0, 2\pi]$ into n directions $\{\theta_i, i = 1, ..., n\}$, resulting in n candidate motions $\{\Delta x_i =$

$(r\cos(\theta_i), r\sin(\theta_i)), i = 1, ..., n\}$. These n small motions serve as motion basis. Larger motion $k\Delta x_i$ can be further added to the pool by estimating the motion matrix $M(k\Delta x_i) = M^k(\Delta x_i)$. The starting position and destination can also be any continuous values, where the encoding to the latent vector is approximated by bilinear interpolation of nearest neighbors on the lattice.

In the experiments, we choose $r = 0.05$ and $n = 100$, and add another set of motion with length 0.025 to enable accurate planning. The system is learned with exponential kernel ($\sigma = 0.3$) as global adjacency to encourage connection of long distance. Figure 4(a) shows planning examples with six settings of motion ranges. Including larger motions accelerates the planning process so that it finishes with less steps. We define one episode to be a success if the distance between the end position and the destination is less than 0.025. We achieve a success rate of $> 99\%$ over $1,000$ episodes for all the six settings.

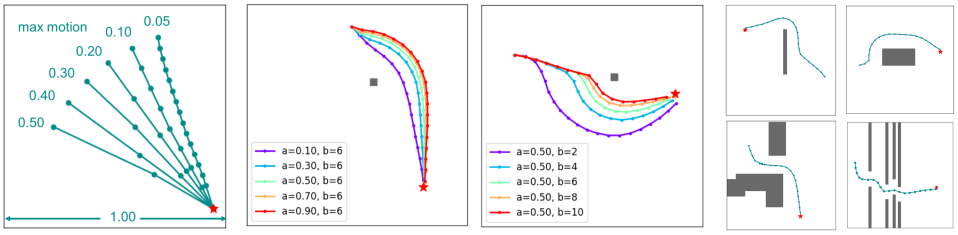

(a) Simple planning (b) Planning with dot obstacle (c) Various obstacles

Figure 4: (a) Planning examples with different motion ranges. Red star represents the destination y and green dots represent the planned position $\{x_0 + \sum_{i=1}^{t} \Delta x_i\}$. (b) Planning examples with a dot obstacle. Left figure shows the effect of changing scaling parameter a, while right figure shows the effect of changing annealing parameter b. (c) Planning example with obstacles mimicking walls, large objects and simple mazes.

The learned system can also perform planning with obstacles, where the global adjacency between the agent's current position and an obstacle serves as a repulsive forces. Specifically, suppose z is an obstacle to avoid, the agent can choose the motion Δx_t at time t by

$$\Delta x_t = \arg\max_{\Delta x \in \mathcal{M}} \left[\langle v(y), M(\Delta x) v_t \rangle - a \langle v(z), M(\Delta x) v_t \rangle^b \right], \tag{15}$$

where a and b are the scaling and annealing parameters. Figure 4(b) shows the planning result with a dot obstacle laid on the direct path between the starting position and destination, with tuning of a and b. We choose $a = 0.5$ and $b = 6$ in subsequent experiments.

Now suppose we have more complicated obstacles $\{z_i\}_{i=1}^m$. They can be included by summing over the kernels of every obstacle $\{a\langle v(z_i), M(\Delta x) v_t \rangle^b\}_{i=1}^m$ and choosing Δx_t at time t by

$$\Delta x_t = \arg\max_{\Delta x \in \mathcal{M}} \left[\langle v(y), M(\Delta x) v_t \rangle - \sum\nolimits_{i=1}^{m} a \langle v(z_i), M(\Delta x) v_t \rangle^b \right]. \tag{16}$$

Figure 4(c) shows some examples, where the obstacles mimicking walls, large objects and simple mazes.

Compared to the potential field method in robotics, here the potential is defined by the adjacencies. Our representation system may be used to implement more sophisticated path planning algorithms such as those based on optimal control. The planned paths may also be distilled into policies.

6 Discussion

The goal of this work is to find a simple and natural model and the associated loss function to learn the grid-like units for navigation, in the hope of contributing to our understanding of the possible computational models of grid cells. Our model consists of a localization sub-model and a motion sub-model. We show that it is possible to learn grid-like units, and the learned model is capable of path integral and path planning. The vector representation is also robust to additive and drop out noises.

REFERENCES

Andrea Banino, Caswell Barry, Benigno Uria, Charles Blundell, Timothy Lillicrap, Piotr Mirowski, Alexander Pritzel, Martin J Chadwick, Thomas Degris, Joseph Modayil, et al. Vector-based navigation using grid-like representations in artificial agents. *Nature*, 557(7705):429, 2018.

Hugh T Blair, Adam C Welday, and Kechen Zhang. Scale-invariant memory representations emerge from moire interference between grid fields that produce theta oscillations: a computational model. *Journal of Neuroscience*, 27(12):3211–3229, 2007.

Yoram Burak and Ila R Fiete. Accurate path integration in continuous attractor network models of grid cells. *PLoS computational biology*, 5(2):e1000291, 2009.

Neil Burgess. Spatial memory: how egocentric and allocentric combine. *Trends in cognitive sciences*, 10(12):551–557, 2006.

Daniel Bush, Caswell Barry, Daniel Manson, and Neil Burgess. Using grid cells for navigation. *Neuron*, 87(3):507–520, 2015.

Krzysztof Choromanski, Mark Rowland, Tamas Sarlos, Vikas Sindhwani, Richard Turner, and Adrian Weller. The geometry of random features. In *International Conference on Artificial Intelligence and Statistics*, pp. 1–9, 2018.

Corinna Cortes and Vladimir Vapnik. Support-vector networks. *Machine learning*, 20(3):273–297, 1995.

Christopher J Cueva and Xue-Xin Wei. Emergence of grid-like representations by training recurrent neural networks to perform spatial localization. *arXiv preprint arXiv:1803.07770*, 2018.

Licurgo de Almeida, Marco Idiart, and John E Lisman. The input–output transformation of the hippocampal granule cells: from grid cells to place fields. *Journal of Neuroscience*, 29(23):7504–7512, 2009.

Inderjit S Dhillon, Yuqiang Guan, and Brian Kulis. Kernel k-means: spectral clustering and normalized cuts. In *Proceedings of the tenth ACM SIGKDD international conference on Knowledge discovery and data mining*, pp. 551–556. ACM, 2004.

Christian F Doeller, Caswell Barry, and Neil Burgess. Evidence for grid cells in a human memory network. *Nature*, 463(7281):657, 2010.

Uğur M Erdem and Michael Hasselmo. A goal-directed spatial navigation model using forward trajectory planning based on grid cells. *European Journal of Neuroscience*, 35(6):916–931, 2012.

Ila R Fiete, Yoram Burak, and Ted Brookings. What grid cells convey about rat location. *Journal of Neuroscience*, 28(27):6858–6871, 2008.

William Fulton and Joe Harris. *Representation theory: a first course*, volume 129. Springer Science & Business Media, 2013.

Marianne Fyhn, Torkel Hafting, Menno P Witter, Edvard I Moser, and May-Britt Moser. Grid cells in mice. *Hippocampus*, 18(12):1230–1238, 2008.

Torkel Hafting, Marianne Fyhn, Sturla Molden, May-Britt Moser, and Edvard I Moser. Microstructure of a spatial map in the entorhinal cortex. *Nature*, 436(7052):801, 2005.

Joshua Jacobs, Christoph T Weidemann, Jonathan F Miller, Alec Solway, John F Burke, Xue-Xin Wei, Nanthia Suthana, Michael R Sperling, Ashwini D Sharan, Itzhak Fried, et al. Direct recordings of grid-like neuronal activity in human spatial navigation. *Nature neuroscience*, 16(9):1188, 2013.

Nathaniel J Killian, Michael J Jutras, and Elizabeth A Buffalo. A map of visual space in the primate entorhinal cortex. *Nature*, 491(7426):761, 2012.

Diederik P Kingma and Jimmy Ba. Adam: A method for stochastic optimization. *arXiv preprint arXiv:1412.6980*, 2014.

Rosamund F Langston, James A Ainge, Jonathan J Couey, Cathrin B Canto, Tale L Bjerknes, Menno P Witter, Edvard I Moser, and May-Britt Moser. Development of the spatial representation system in the rat. *Science*, 328(5985):1576–1580, 2010.

Daniel D Lee and H Sebastian Seung. Learning the parts of objects by non-negative matrix factorization. *Nature*, 401(6755):788, 1999.

Bruce L McNaughton, Francesco P Battaglia, Ole Jensen, Edvard I Moser, and May-Britt Moser. Path integration and the neural basis of the'cognitive map'. *Nature Reviews Neuroscience*, 7(8): 663, 2006.

Tomas Mikolov, Ilya Sutskever, Kai Chen, Greg Corrado, and Jeffrey Dean. Distributed representations of words and phrases and their compositionality. In *Proceedings of the 26th International Conference on Neural Information Processing Systems - Volume 2*, NIPS'13, pp. 3111–3119, 2013.

Andrew Y Ng, Michael I Jordan, and Yair Weiss. On spectral clustering: Analysis and an algorithm. In *Advances in neural information processing systems*, pp. 849–856, 2002.

Ali Rahimi and Benjamin Recht. Random features for large-scale kernel machines. In *Advances in neural information processing systems*, pp. 1177–1184, 2008.

Sam T. Roweis and Lawrence K. Saul. Nonlinear dimensionality reduction by locally linear embedding. *SCIENCE*, 290:2323–2326, 2000.

Francesca Sargolini, Marianne Fyhn, Torkel Hafting, Bruce L McNaughton, Menno P Witter, May-Britt Moser, and Edvard I Moser. Conjunctive representation of position, direction, and velocity in entorhinal cortex. *Science*, 312(5774):758–762, 2006.

Roland Siegwart, Illah Reza Nourbakhsh, Davide Scaramuzza, and Ronald C Arkin. *Introduction to autonomous mobile robots*. MIT press, 2011.

Sameet Sreenivasan and Ila Fiete. Grid cells generate an analog error-correcting code for singularly precise neural computation. *Nature neuroscience*, 14(10):1330, 2011.

Hanne Stensola, Tor Stensola, Trygve Solstad, Kristian Frøland, May-Britt Moser, and Edvard I Moser. The entorhinal grid map is discretized. *Nature*, 492(7427):72, 2012.

Albert Tsao, Jørgen Sugar, Li Lu, Cheng Wang, James J Knierim, May-Britt Moser, and Edvard I Moser. Integrating time from experience in the lateral entorhinal cortex. *Nature*, 561(7721):57, 2018.

H Durrant Whyte. Simultaneous localisation and mapping (slam): Part i the essential algorithms. *Robotics and Automation Magazine*, 2006.

Michael M Yartsev, Menno P Witter, and Nachum Ulanovsky. Grid cells without theta oscillations in the entorhinal cortex of bats. *Nature*, 479(7371):103, 2011.

A PROOF FOR SECTION 5.1.3

Theorem 1. *Let $e(x) = (e^{i\langle a_j, x\rangle}, j = 1, 2, 3)^\top$, and a_1, a_2, a_3 are three 2D vectors so that the angle between a_i and a_j is $2\pi/3$ for $\forall i \neq j$ and $|a_j| = 2\sqrt{\alpha}$ for $\forall j$. Let C be any 3×3 complex matrix such that $C^*C = I$. Then $v(x) = Ce(x)/\sqrt{3}$, $M(\Delta x) = C\mathrm{diag}(e(\Delta x))C^*$ satisfy equation 1 $\forall x, \Delta x$, and equation 8 $\forall x, y$, approximately for small $|x - y|$.*

Proof. $(a_j, j = 1, 2, 3)$ forms a tight frame in the 2D space, in that for any vector x in 2D, $\sum_{j=1}^{3} \langle x, a_j\rangle^2 \propto |x|^2$.

Since $C^*C = I$, we have

$$\begin{aligned}
\langle v(x), v(y)\rangle &= v(x)^* v(y) && (17)\\
&= \frac{1}{3} e(x)^* C^* C e(y) && (18)\\
&= \frac{1}{3} \sum_{j=1}^{3} e^{i\langle a_j, y-x\rangle}. && (19)
\end{aligned}$$

Then we have

$$\begin{aligned}
\mathrm{RE}(\langle v(x), v(y)\rangle) &= \frac{1}{3} \sum_{j=1}^{3} \cos(\langle a_j, y - x\rangle) && (20)\\
&\approx \frac{1}{3} \sum_{j=1}^{3} (1 - \langle a_j, y - x\rangle^2/2) && (21)\\
&= \frac{1}{3} \left(3 - \sum_{j=1}^{3} \langle a_j, y - x\rangle^2/2 \right) && (22)\\
&= \frac{1}{3}(3 - 3\omega^2 |y - x|^2/4) && (23)\\
&= 1 - \alpha |y - x|^2, && (24)
\end{aligned}$$

where $\omega = |a_j| = 2\sqrt{\alpha}$.

The self motion from $v(x)$ to $v(x + \Delta x)$ is

$$\begin{aligned}
v(x + \Delta x) &= Ce(x + \Delta x) && (25)\\
&= CD(\Delta x)e(x) && (26)\\
&= CD(\Delta x)C^* v(x) && (27)\\
&= M(\Delta x)v(x), && (28)
\end{aligned}$$

where $D(\Delta x) = \mathrm{diag}(e^{i\langle a_j, \Delta x\rangle}, j = 1, 2, 3)$. □

If $K > 1$ and block size $= 6$, for a translation invariance function $A(x, y)$, it can be approximated by Fourier expansion

$$\begin{aligned}
A(x, y) &= f(|x - y|) && (29)\\
&= \langle v(x), v(y)\rangle && (30)\\
&\approx \sum_{k=1}^{K} \sum_{j=1}^{3} e^{i\langle a_{kj}, y-x\rangle}/3 && (31)\\
&= \sum_{k=1}^{K} \langle v^{(k)}(x), v^{(k)}(y)\rangle. && (32)
\end{aligned}$$

That is, we can fit the multiple blocks together.

B HEXAGON GRID PATTERNS AND METRICS

B.1 LEARNED SINGLE BLOCK UNITS WITH DIFFERENT BLOCK SIZES

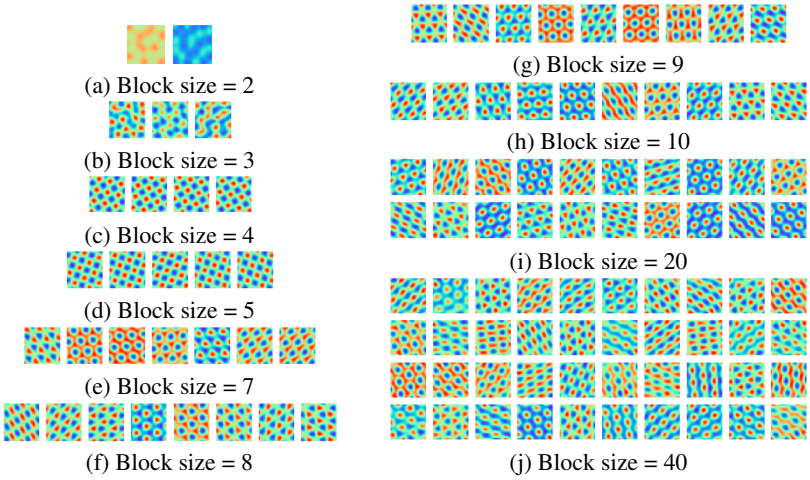

Figure 5: Response maps of learned single block units with different block sizes

Figure 5 displays the response maps of the learned single block units with different block sizes. For block sizes 4 and 5, the learned maps show square lattice patterns. For block sizes greater than or equal to 6, the learned maps show hexagon lattice patterns.

B.2 LEARNED MULTIPLE BLOCK UNITS AND METRICS

B.2.1 WITH DIFFERENT BLOCK SIZES

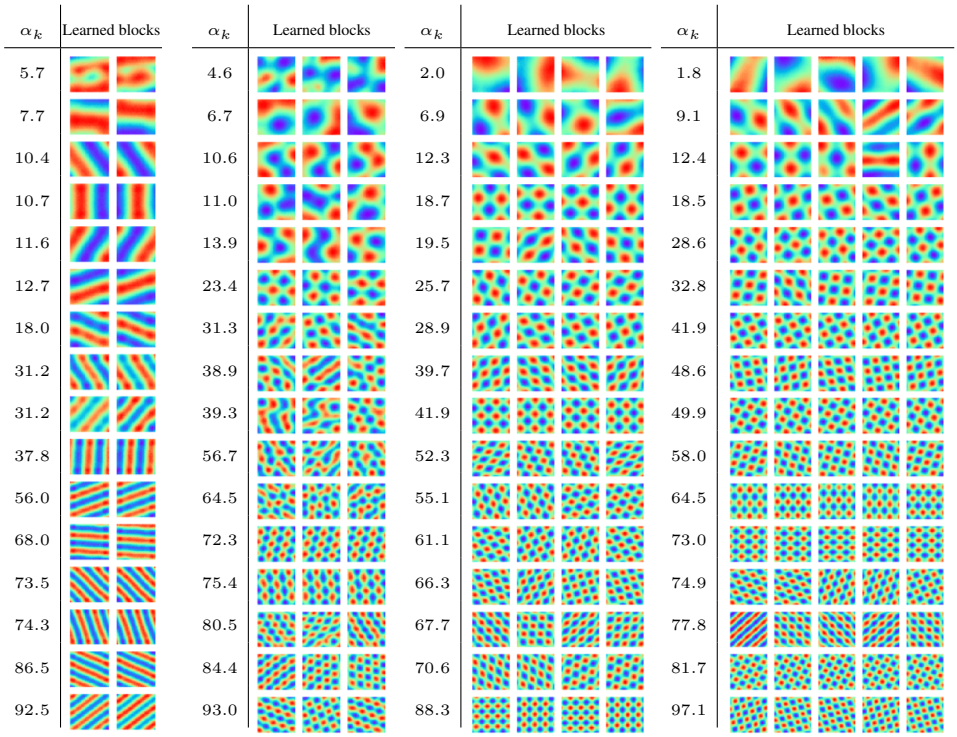

(a) Block size = 2 (b) Block size = 3 (c) Block size = 4 (d) Block size = 5

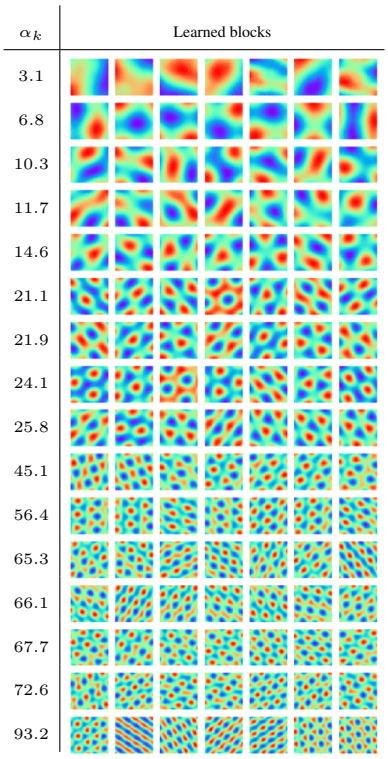

(e) Block size = 7

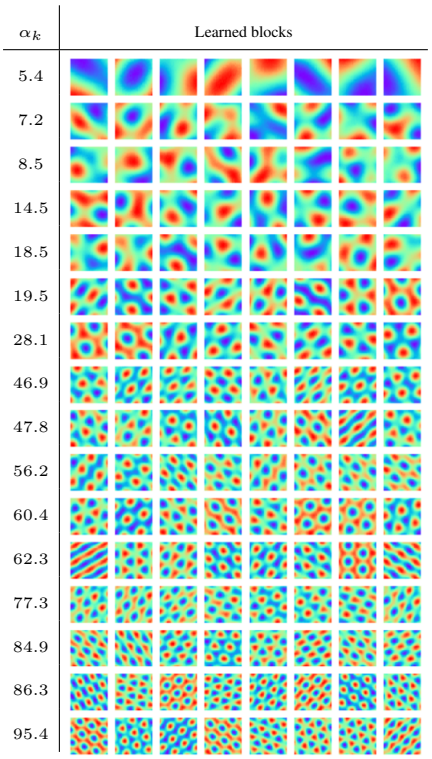

(f) Block size = 8

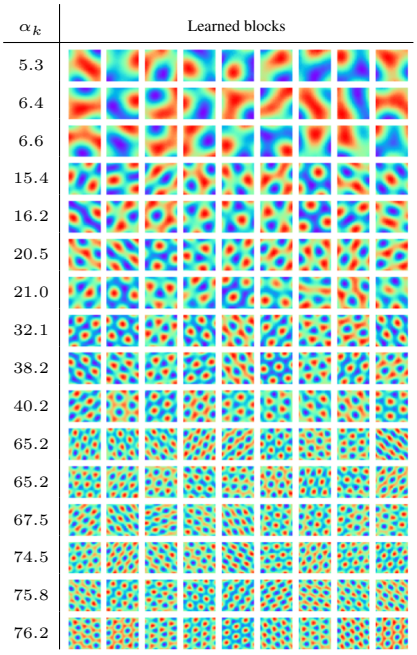

(g) Block size = 9

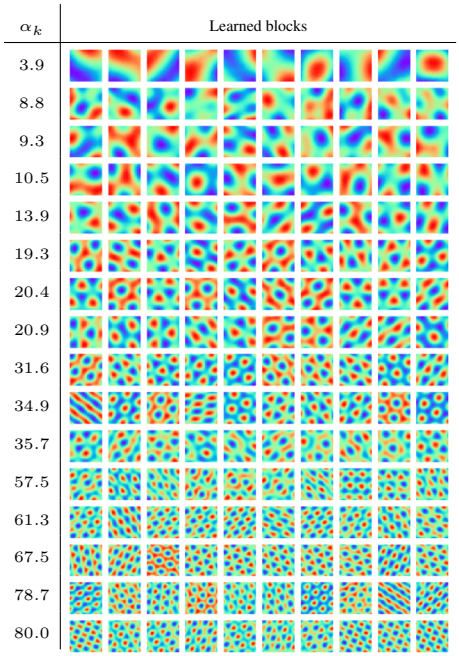

(h) Block size = 10

Figure 6: Learned multiple block units and metrics with different block sizes

Figure 6 displays the response maps of the multiple block units with different block sizes. The metrics of the multiple blocks are learned automatically.

B.2.2 WITH DIFFERENT SHAPES OF AREA

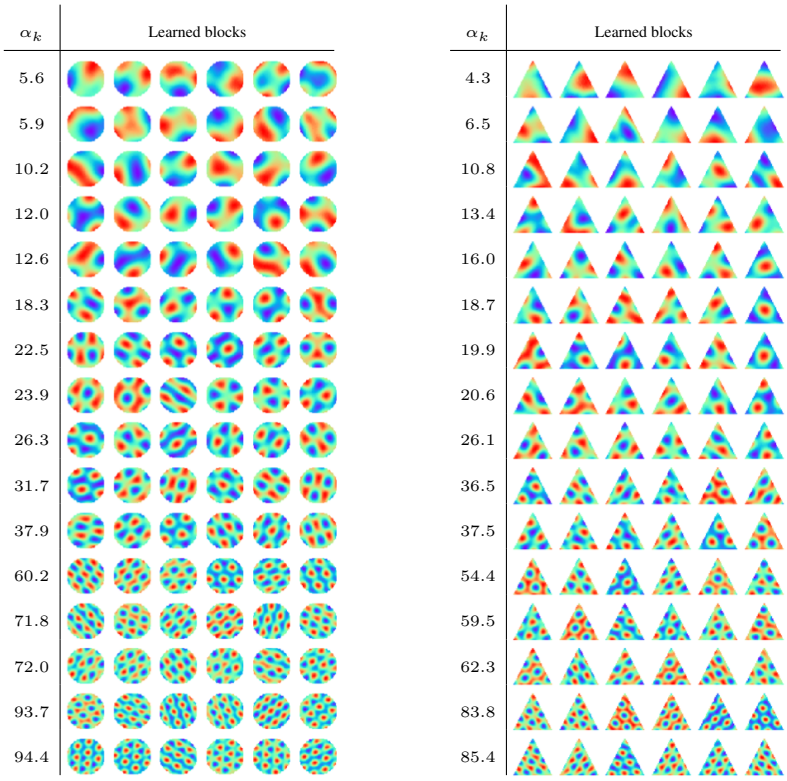

(a) Circular area (b) Triangular area

Figure 7: Learned multiple block units and metrics with different shapes of the area

Figure 7 displays the response maps of the multiple block units with different shapes of the area, such as circle and triangle.

B.3 QUANTITATIVE ANALYSIS OF SPATIAL ACTIVITY

We assess the spatial activity of the learned units quantitatively using measures adopted from the neuroscience literature. Specifically, we quantify the hexagonal regularity of the grid-like patterns using the gridness score (Langston et al. (2010); Sargolini et al. (2006)). The measure is derived from the spatial autocorrelogram of each unit's response map. A unit is classified as a grid cell if its gridness score is larger than 0. For those units that are classified as grid cells, grid scale and orientation can be further derived from the autocorrelogram following Sargolini et al. (2006). Figure 8(a) summarizes the results. 76 out of 96 learned units are classified as grid cells. Most units with large learned α_k are classified as grid cells, while those units with small α_k are not due to lack of a full period of hexagonal patterns. The grid scales and orientations vary among units, while remain similar within each block. We show the histograms of the grid orientations and scales in figures 8(b) and 8(c) respectively. Moreover, we average the grid scales within each block and make the scatter plot of the averaged grid scales and the learned $1/\sqrt{\alpha_k}$ in figure 8(d). Interestingly, the grid scale is nicely proportional to the learned $1/\sqrt{\alpha_k}$.

B.4 ABLATION STUDIES

We conduct ablation studies to assess various assumptions in our model.

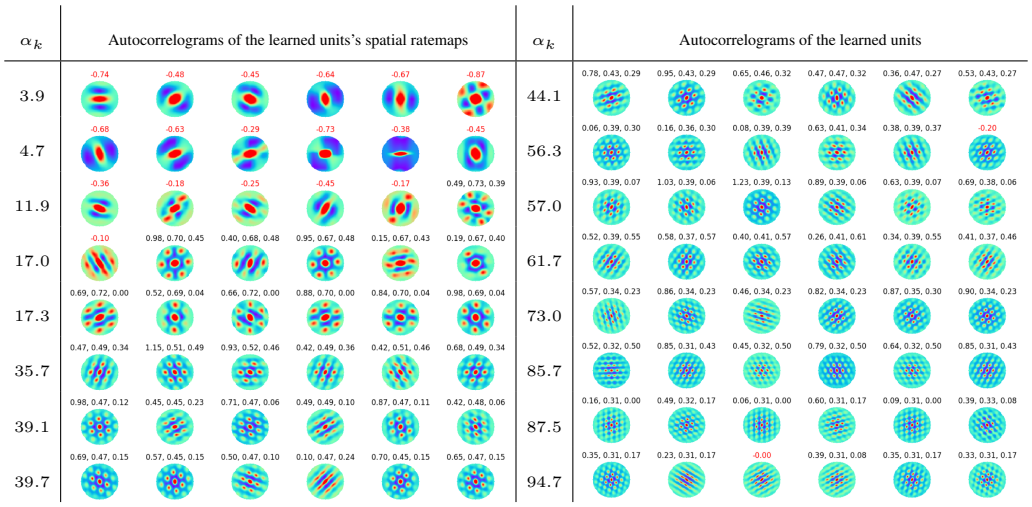

(a) Autocorrelograms of the learned units' response maps.

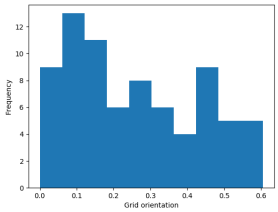

(b) Histogram of grid orientations

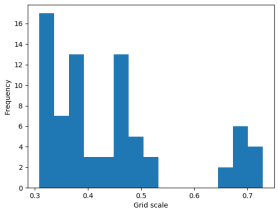

(c) Histogram of grid scales

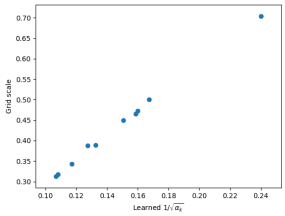

(d) Scatter plot of grid scales and learned $1/\sqrt{\alpha_k}$

Figure 8: (a) Autocorrelograms of the learned units' response maps. Gridness scores are calculated based on the autocorrelograms. A unit is classified as a grid cell if the gridness score is larger than 0. The gridness score is shown in red color if a unit fails to be classified as a grid cell. For those units that are classified as grid cells, gridness score, scale and orientation are listed sequentially in black color. Orientation is computed using a camera-fixed reference line ($0°$) and in counter-clockwise direction. (Zooming in on pdf file is recommended.) (b) Histogram of grid orientations. (c) Histogram of grid scales. (d) Scatter plot of averaged grid scales within each block and the corresponding learned $1/\sqrt{\alpha_k}$.

B.4.1 Loss terms

We learn v and M with multiple blocks by minimizing equation 12, which consists of (1) a localization loss with global adjacency, (2) a localization loss with local adjacency, and (3) a motion loss. Figure 9 shows the learned units when using only some of the components. Grid-like patterns do not emerge if using only the localization loss with global adjacency, or only the localization loss with local adjacency. If using only the motion loss, the motion equation is approximately satisfied at the beginning of training, since both v and M are initialized from small values that are close to 0. The system cannot be learned without an extra term to push $v(x)$ apart from each other. Figure 9(c) shows the learned units using the localization loss with global adjacency and the motion loss, leaving out the local adjacency. Grid-like patterns still emerge (also some strip-like patterns), although less obvious than the ones learned using the full loss.

B.4.2 Assumptions of motion matrix

In another ablation study, we drop the quadratic parametrization by β coefficients and the block diagonal assumption of the motion matrix. A separate motion matrix $M(\Delta x)$ is learned for each displacement Δx, and $v(x)$ is assumed to be a single block. We use either the local or global adjacency in the localization model. The results are shown in Figure 10. With the local adjacency, the

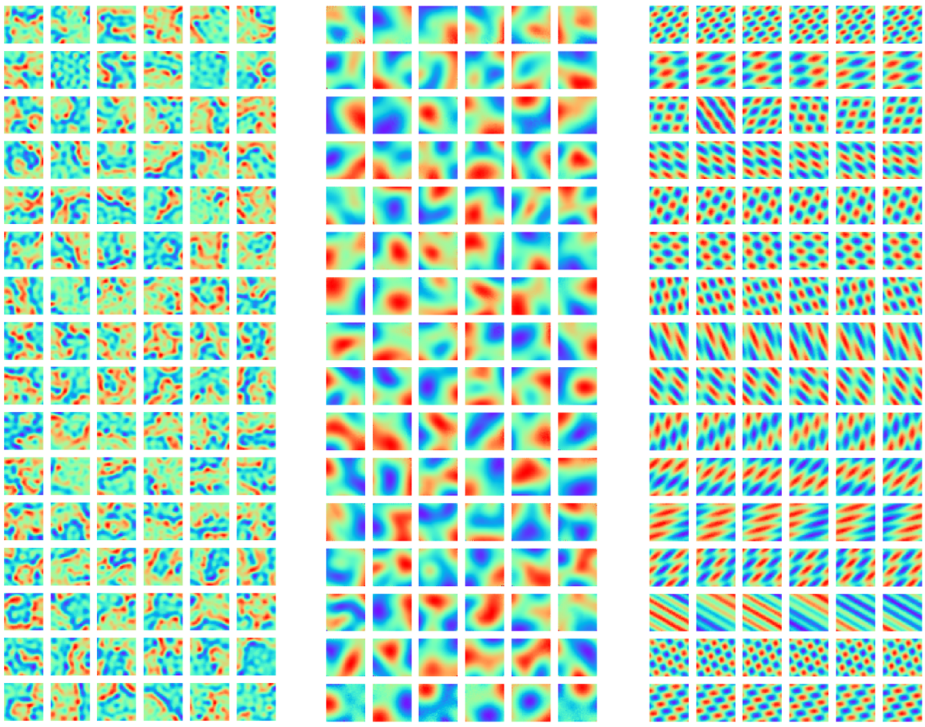

(a) Using only localization loss with global adjacency

(b) Using only localization loss with local adjacency

(c) Using global (but not local) adjacency and motion loss.

Figure 9: Ablation study of the components in the training loss. (a) Learn the model using only the localization loss with global adjacency. (b) Learn the model using only the localization loss with local adjacency. (c) Using global adjacency and motion loss, leaving out local adjacency.

setting is similar to the one of learning single block, except that the parametrization of $M(\Delta x)$ is dropped. As shown in figure 10(a), the learned units resemble the one learned with parametrized $M(\Delta x)$, but when block size is large, the grid-like patterns are less obvious. With the global adjacency, grid-like patterns do not emerge any more.

C MODELING EGOCENTRIC MOTION

The model can be generalized to handle egocentric motion that involves head direction.

C.1 COUPLING TWO GRID SYSTEMS

The egocentric motion consists of angular velocity in the change of head direction and the spatial velocity along the current head direction. We couple two grid systems, one for head direction and the other for the spatial position. For notational simplicity, we put the "hat" notation on top of v and M notation to denote the vector and matrix for the head direction.

Specifically, the agent has a head direction θ, which may change over time. The agent moves along its head direction with scalar motion. We can discretize the range of θ, $[0, 2\pi]$, into $\hat{N}$ equally spaced values $\{\theta_i, i = 1, ..., \hat{N}\}$, and introduce a vector representation of self-direction. That is, the agent represents its self-direction by a $\hat{d}$-dimensional hidden vector $\hat{v}(\theta)$.

C.1.1 MOTION SUB-MODEL

Suppose at a position x, the agent has a head direction θ. The self-motion is decomposed into (1) a scalar motion δ along the head direction θ and then (2) a head direction rotation $\Delta\theta$. The self-motion

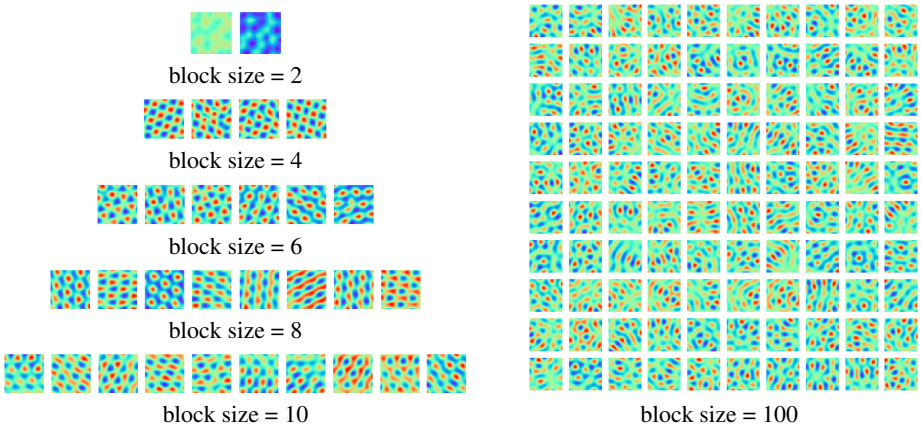

(a) With local adjacency: scaling parameter $\alpha = 72$

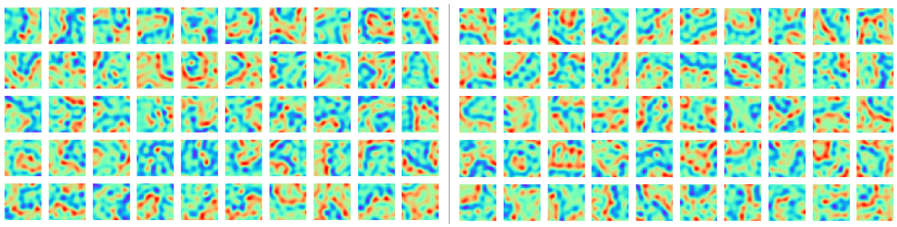

(b) With global adjacency: Gaussian kernel with $\sigma = 0.08$

Figure 10: Learned units by dropping the parametrization and the block diagonal assumption of the motion matrix $M(\Delta x)$.

$\Delta x = (\delta \cos\theta, \delta \sin\theta)$. We assume

$$\hat{v}(\theta + \Delta\theta) = \hat{M}(\Delta\theta)\hat{v}(\theta), \tag{33}$$

$$v(x + \Delta x) = M(\delta, \hat{v}(\theta))v(x), \tag{34}$$

where $\hat{M}(\Delta\theta)$ is a $\hat{d} \times \hat{d}$ matrix that depends on $\Delta\theta$, and $M(\Delta\theta, \hat{v}(\theta))$ is a $d \times d$ matrix that depends on δ and $\hat{v}(\theta)$. $\hat{M}(\Delta\theta)$ is the matrix representation of the head direction rotation $\Delta\theta$, while $M(\delta, \hat{v}(\theta))$ is the matrix representation of scalar motion δ along the direction θ.

We can model $M(\delta, \hat{v}(\theta))$ by an attention (or selection) mechanism:

$$p_i = \frac{\langle \hat{v}(\theta), \hat{v}(\theta_i) \rangle^b}{\sum_{i=1}^{\hat{N}} \langle \hat{v}(\theta), \hat{v}(\theta_i) \rangle^b}, \tag{35}$$

$$M(\delta, \hat{v}(\theta)) = \sum\nolimits_{i=1}^{\hat{N}} p_i M^{(i)}(\delta), \tag{36}$$

where $M^{(i)}(\delta)$ is the matrix representation of scalar motion δ given the head direction θ_i. The inner product $\langle \hat{v}(\theta), \hat{v}(\theta_i) \rangle$, which informs the angular distance between θ and θ_i, serves as the attention weights. b is an annealing (inverse temperature) parameter. If $b \to \infty$, $p = (p_i, i = 1, ..., \hat{N})$ becomes a one-hot vector for selection. We can further assume that $\hat{M}(\Delta\theta)$ and $M^{(i)}(\delta)$ are block diagonal, and learn a parametric model for each of them by the second order Taylor expansion in $\Delta\theta$ and δ respectively.

C.1.2 Localization sub-model

For the localization sub-model, we define the adjacency measures of self-direction and self-position separately. Let $\hat{A}(\theta_1, \theta_2)$ be the adjacency measure between two directions θ_1 and θ_2 such that $\hat{A}(\theta_1, \theta_2) = \hat{f}(|\theta_1 - \theta_2|)$. We use von Mises kernel $\hat{f}(r) = \exp((\cos(r) - 1)/\sigma^2)$, where $\hat{f}(0) = 1$. For adjacency measure $A(x, y)$ between self-positions x and y, we keep it the same as described in section 3.2.

C.1.3 LOSS FUNCTION FOR LEARNING

For learning the system, we can first learn $\hat{v}$ and $\hat{M}$ (or the coefficients that parametrize $\hat{M}$) by minimizing

$$\mathbb{E}_{\theta_1,\theta_2}\left[(\hat{A}(\theta_1,\theta_2) - \langle \hat{v}(\theta_1), \hat{v}(\theta_2)\rangle)^2\right] + \lambda \mathbb{E}_{\theta,\Delta\theta}\left[\|\hat{v}(\theta+\Delta\theta) - \hat{M}(\Delta\theta)\hat{v}(\theta)\|^2\right], \tag{37}$$

and then we learn v and M (or the coefficients that parametrize M) by minimizing equation 12.

C.2 LEARNED UNITS FOR SELF-DIRECTION AND SELF-POSITION

Figure 11 shows a result of learning such an egocentric motion model by displaying the response curves of the learned units in the head direction system, $\hat{v}(\theta)$, for $\theta \in [0, 2\pi]$, as well as the response maps of the learned multiple block units in the self-position system, $v(x)$, for $x \in [0, 1]^2$.

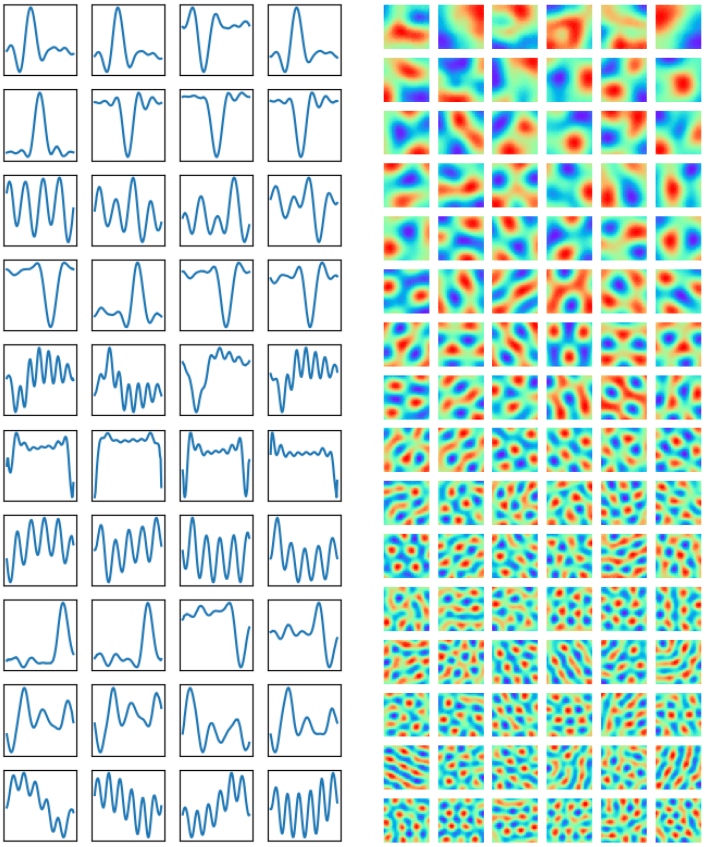

(a) (b)

Figure 11: (a) Response curves of learned units in the head direction model, $\hat{v}(\theta)$. Each block shows the units belonging to the same sub-vector in the model. The horizontal axis represents the angle within a range of [0, 2π], while the vertical axis indicates the values of responses. (b) Response maps of the learned multiple block units of the self-position model, $v(x)$, for $x \in [0, 1]^2$.

C.3 CLOCK AND TIMESTAMP

We may re-purpose the head direction system as a clock, by interpreting $\theta \in [0, 2\pi]$ as the time on a clock, and $\hat{v}(\theta)$ as a time2vec, or timestamp for events happening over time. This may be related to the recent neuroscience observations in Tsao et al. (2018).

D ERRORS

D.1 ERROR CORRECTION

Unlike commonly used embedding in machine learning, here we embed a 2D position into a high-dimensional space, and the embedding is a highly distributed representation or population code. The advantage of such a redundant code is in it's tolerance to errors. We show that the learned system is tolerant to various errors of units. Specifically, in both path integral and path planning tasks, at every time step t, we randomly add (1) Gaussian noises or (2) drop out masks to the hidden units and see if the system can still perform the tasks well. We find that the decoding-encoding process (DE) is important for error correction. That is, at each time step t, given the noisy hidden vector v_t, we decode it to $x_t = \arg\max_x \langle v_t, v(x) \rangle$ and then re-encode it to the hidden vector $v(x_t)$.

Table 1 shows the error correction results tested on path integral and path planning tasks. Each number is averaged over $1,000$ episodes. We compute the overall standard deviation of $\{v(x)\}$ for all x and treat it as the reference standard deviation (s) for the Gaussian noise. For drop out noise, we set a percentage to drop at each time step. With the decoding-encoding process, the system is quite robust to the Gaussian noise and drop out error, and the system still works even 70% units are silenced at each step.

	Path integral: MSE					Path planning: success rate				
Noise type	$1s$	$0.75s$	$0.5s$	$0.25s$	$0.1s$	$1s$	$0.75s$	$0.5s$	$0.25s$	$0.1s$
Gaussian (DE)	1.687	1.135	0.384	0.017	0	0.928	0.959	0.961	0.977	0.985
Gaussian	6.578	2.999	1.603	0.549	0.250	0.503	0.791	0.934	0.966	0.982
Noise type	70%	50%	30%	10%	5%	70%	50%	30%	10%	5%
Dropout (DE)	2.837	1.920	1.102	0.109	0.013	0.810	0.916	0.961	0.970	0.978
Dropout	19.611	16.883	14.137	3.416	0.602	0.067	0.186	0.603	0.952	0.964

Table 1: Error correction results on the vector representation. The performance of path integral is measured by mean square error between predicted locations and ground truth locations; while for path planning, the performance is measured by successful rate. Experiments are conducted using several noise levels: Gaussian noise with different standard deviations in terms of the reference standard deviation s and drop out mask with different percentages. DE means implementing decoding-encoding process when performing the tasks.

D.2 NOISY SELF-MOTION INPUT

Besides adding noises to the hidden units, we also experiment with adding noises to the self-motion Δx, and compare the performance of path integral with the one performed in the original 2D coordinates. Specifically, at each time step, we add Gaussian noises to the self-motion Δx. For path integral, we compute the mean square error between the predicted locations and ground truth locations. Besides, we also compute the predicted locations using the 2D coordinates with the noisy self-motions. Its mean square error serves as the reference error. Table 2 shows the result, indicating that the error of the learned system is close to the error in the original 2D coordinates, i.e., our system does not blow up the noise.

Standard deviation	1.2	0.9	0.6	0.3
Learned system	6.020	4.382	3.000	1.422
Reference	5.852	4.185	2.873	1.315

Table 2: Path integral results with noises in the self-motion. Performance is measured by mean square error (MSE) between the predicted locations and ground truth locations in the path integral task. Noises are added to self-motions Δx by several noise levels: Gaussian noise with different standard deviations in terms of number of grids. Reference MSE is computed by path integral in 2D coordinates.

E 3D ENVIRONMENT

The system can be generalized to 3D environments. Specifically, we assume the agent navigates within a domain $D = [0, 1] \times [0, 1] \times [0, 1]$, which is discretized into a $40 \times 40 \times 40$ lattice. We learn a parametric model for motion matrix M by a residual form $M = I + \tilde{M}(\Delta x)$. To estimate $\tilde{M}(\Delta x)$ more precisely, we parametrize each element of $\tilde{M}(\Delta x)$ as a cubic function of $\Delta x = (\Delta x_1, \Delta x_2, \Delta x_3)$.

A batch of 200,000 examples of (x, y) and $(x, \Delta x_t, t = 1, ..., T)$ is sampled online at every iteration for training. We use 16 blocks of units with block size 6 and choose Gaussian kernel ($\sigma = 0.08$) as the adjacency measure. Figure 12 shows four learned 3D units, where the grid-like patterns emerge. We also show that the learned system can perform path integral, simple path planning and planning with a cuboid obstacle tasks well.

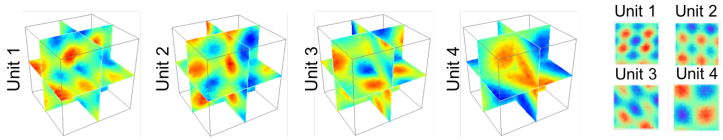

Figure 12: Four examples of learned 3D units from different blocks. Left four figures show the 3D visualization, while the rightmost figure shows the patterns of a slice of every unit.

E.1 3D PATH INTEGRAL

Please see figure 13.

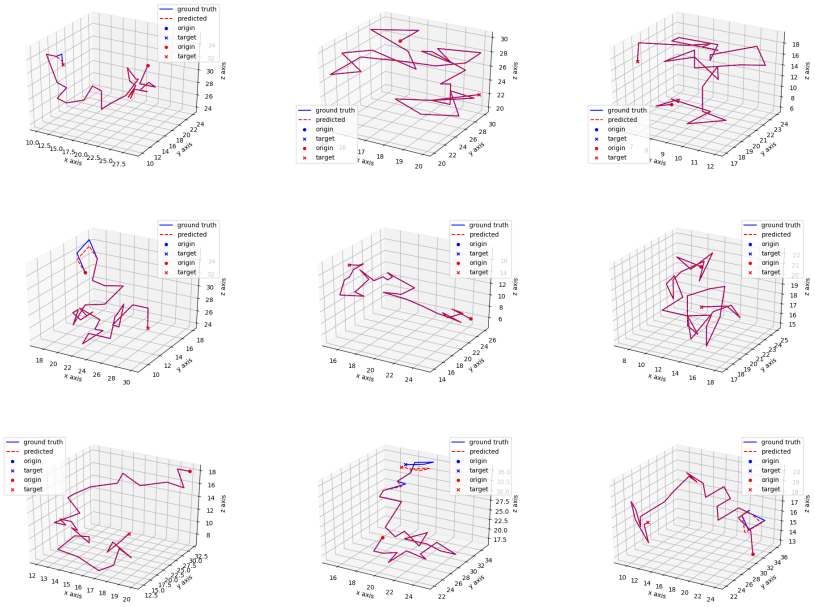

Figure 13: Examples of 3D path integral with duration $\tilde{T} = 30$.

E.2 3D PATH PLANNING

Please see figure 14.

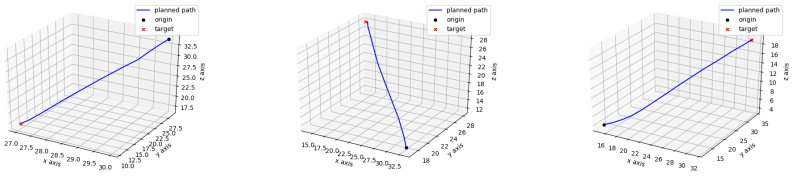

Figure 14: Examples of 3D simple path planning, where the agent is capable of planning a direct trajectory.

E.3 3D PATH PLANNING WITH OBSTACLES

Please see figure 15.

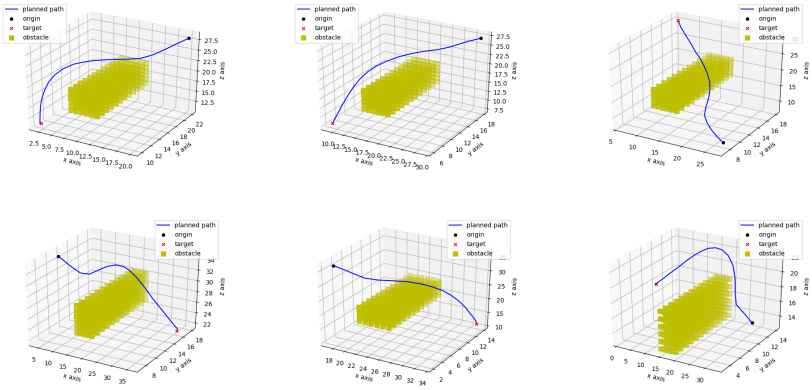

Figure 15: Examples of 3D path planning with a cuboid obstacle.